



RESEARCH LETTER

10.1002/2016GL070501

Key Points:

- A sole NGCU iron source underestimates observed EUC iron
- A sole NGCU iron is subject to high dilution and scavenging
- Additional NICU iron may explain timing and intensity of blooms in the EEP

Supporting Information:

- Supporting Information S1

Correspondence to:

L. Menviel,
l.menviel@unsw.edu.au

Citation:

Qin, X., L. Menviel, A. Sen Gupta, and E. van Sebille (2016), Iron sources and pathways into the Pacific Equatorial Undercurrent, *Geophys. Res. Lett.*, *43*, 9843–9851, doi:10.1002/2016GL070501.

Received 18 JUL 2016

Accepted 12 SEP 2016

Accepted article online 13 SEP 2016

Published online 29 SEP 2016

Iron sources and pathways into the Pacific Equatorial Undercurrent

Xuerong Qin¹, Laurie Menviel¹, Alex Sen Gupta¹, and Erik van Sebille^{1,2}

¹Climate Change Research Centre and ARC Centre of Excellence on Climate System Science, University of New South Wales, Sydney, New South Wales, Australia, ²Grantham Institute and Department of Physics, Imperial College London, London, UK

Abstract Using a novel observationally constrained Lagrangian iron model forced by outputs from an eddy-resolving biogeochemical ocean model, we examine the sensitivity of the Equatorial Undercurrent (EUC) iron distribution to EUC source region iron concentrations. We find that elevated iron concentrations derived from New Guinea Coastal Undercurrent (NGCU) alone is insufficient to explain the high concentrations observed in the EUC. In addition, due to the spread in transit times, interannual NGCU iron pulses are scavenged, diluted, or eroded, before reaching the eastern equatorial Pacific. With an additional iron source from the nearby New Ireland Coastal Undercurrent, EUC iron concentrations become consistent with observations. Furthermore, as both the New Guinea and New Ireland Coastal Undercurrents strengthen during El Niño, increased iron input into the EUC can enhance the iron supply into the eastern equatorial Pacific. Notably, during the 1997/1998 El Niño, this causes a simulated 30% iron increase at a 13 month lag.

1. Introduction

Shelf sediments in the western Pacific are a primary source of dissolved iron to the Equatorial Undercurrent (EUC). This rapid current, which extends across the Pacific, transports iron eastward that is upwelled in the eastern equatorial Pacific (EEP). The delivery of iron to this iron-limited part of the ocean enhances primary production [Christian *et al.*, 2002; Gorgues *et al.*, 2010; Ryan *et al.*, 2006; Slemons *et al.*, 2009, 2010; Vichi *et al.*, 2008]. Most western Pacific iron is thought to enter the water column from the reductive mobilization of iron through sediment resuspension and nonreductive sediment dissolution on the continental shelf with lesser contributions from hydrothermal and riverine sources [Gordon *et al.*, 1997; Johnson and McPhaden, 1999; Mackey *et al.*, 2002; Slemons *et al.*, 2009, 2010; Radic *et al.*, 2011; Labatut *et al.*, 2014]. Iron is carried into the EUC by the low-latitude western boundary currents (LLWBCs) that interact with the western Pacific sediment shelves (Figure S1). While there is general agreement on the importance of the western Pacific as a primary source of iron [Coale *et al.*, 1996; Mackey *et al.*, 2002; Slemons *et al.*, 2012, 2010; Wells *et al.*, 1999], the combination of the various potential regional sources that supply the EUC iron is uncertain due to sparse measurements. The best studied of these sources is the New Guinea Coastal Undercurrent (NGCU), where repeated measurements off Papua New Guinea indicate elevated trace metal concentrations of lithogenic origin [Mackey *et al.*, 2002; Slemons *et al.*, 2010].

For various reasons, there has been less focus on the role of the other LLWBCs: the Mindanao Current (MC) and the New Ireland Coastal Undercurrent (NICU) as potential iron sources. Measurements from the western Pacific [Mackey *et al.*, 2002] showed that at 5°N and 155°E, dissolved iron concentrations were 2–3 times lower than EUC measurements, suggesting that northwest tropical waters feeding the EUC have a low iron content. However, these low iron measurements were conducted in the open ocean, far from the continental margin and the MC. The NICU flows past a number of potential hydrothermal iron sources, particularly near the island of Lihir, where there is active venting within Louise Harbour (Figure S1). These hydrothermal sources are well separated from the NGCU, and so iron from these sources can only be transported by the NICU [Pichler *et al.*, 1999]. The lack of measurements around these regions mean that the MC and NICU cannot be ruled out as possible entry points for subsurface iron that feeds into the EUC.

Following decreases in primary production during the strong 1997/1998 El Niño, an exceptionally large bloom occurred in the central and eastern equatorial Pacific during the transition to La Niña in 1998 [Chavez *et al.*, 1999]. A possible explanation is that El Niño–Southern Oscillation (ENSO)-related circulation changes in the western tropical Pacific at the peak of the El Niño may have altered the (micro)nutrient composition of the EUC source waters sufficiently to modulate productivity in the central and eastern equatorial

Pacific 9–13 months later [Gorgues *et al.*, 2010; Ryan *et al.*, 2006; Slemons *et al.*, 2009]. Ryan *et al.* [2006] hypothesized that the NGCU intensified during the 1997 El Niño developing meanders and eddies that enhanced coupling of the Papua New Guinea shelf to the EUC, thereby increasing the NGCU iron content. This could subsequently lead to a greater delivery of iron to the eastern equatorial Pacific, thereby facilitating large blooms. To examine this proposed mechanism linking western and eastern Pacific iron variabilities, Gorgues *et al.* [2010] simulated a time-varying NGCU iron concentration using the coupled ocean biogeochemical model Nucleus for European Modelling of the Ocean (NEMO). They found that setting the iron source proportional to the NGCU speed in the source region did not change the intensity or initiation time of EEP blooms compared to a time constant iron concentration at the source. Indeed, anomalously high iron concentrations propagating via the EUC pathway were rapidly reduced through scavenging before reaching the upwelling region. It therefore remains unclear whether interannual variations in the NGCU or other iron sources can impact iron levels and productivity in the EEP upwelling zone.

Here we developed an iron-tracking Lagrangian model constrained by available observations to examine the potential sources of iron to the EUC and to understand the importance of dilution, scavenging, and biological processes on iron transport at eddy-resolving scales. We focused on locating potential iron sources rather than resolving the mechanisms of iron input into the water column.

2. Models and Methods

Lagrangian model particles are integrated using the Connectivity Modelling System [Paris *et al.*, 2013]. Velocity fields used to advect Lagrangian particles are taken from the Ocean Forecasting Australia Model version (OFAM3) [Oke *et al.*, 2012], described in detail in Qin *et al.* [2015]. The biogeochemical fields used in the iron model parameterizations are based on three-dimensional daily-averaged output from the Whole Ocean Model with Biogeochemistry and Trophic-dynamics (WOMBAT) biogeochemical model coupled to OFAM3. Validation of OFAM3 tropical Pacific circulation is described in Text S2 in the supporting information.

The sparsity of dissolved iron measurements [Tagliabue *et al.*, 2015], limited knowledge of iron source locations and release magnitudes [Aumont *et al.*, 2015], and uncertainty around processes associated with iron scavenging [Tagliabue *et al.*, 2015] lead to a limited ability to realistically model the equatorial Pacific iron cycle. As a result, many of state-of-the-art global ocean biogeochemical models are unable to reproduce aspects of the observed iron distribution [Tagliabue *et al.*, 2015].

To better constrain the importance of different iron sources in the western equatorial Pacific and the impact of scavenging on iron transport to the eastern part of the basin, we developed a Lagrangian iron model and conducted a series of sensitivity experiments, in which we alter exogenous source inputs of iron and compare simulated concentrations along the equatorial Pacific with available iron observations. In Lagrangian form, the equation for the evolution of iron along a Lagrangian particle trajectory is given by

$$\frac{D\mathbf{Fe}}{Dt} = Fe_{src} + Fe_{reg} - Fe_{phy} - Fe_{scav} \quad (1)$$

in which iron change $D\mathbf{Fe}/Dt$ (nM d^{-1}) is the sum of the effects of exogenous inputs (Fe_{src}), remineralization (Fe_{reg}), uptake by phytoplankton (Fe_{phy}), and scavenging (Fe_{scav}). Iron changes due to remineralization of organic matter (Fe_{reg}) are 2 orders of magnitude lower in the EUC compared to the other terms, and their contribution to the mean EUC iron concentration in the experiments with high iron concentrations (e.g., NGCU-HIGH in Table 1) is 0.03 nM compared to a reduction of 5 to 7 nM from scavenging and dilution. See Text S7 for further discussion on the role of remineralization. Iron scavenging Fe_{scav} is of primary importance for the evolution of iron from the source regions to the EEP via the EUC. In our model, iron is parameterized as in Galbraith *et al.* [2010]:

$$Fe_{scav} = k_{Fe}^{org} \left(\frac{Det_f}{w_{sink}} \right)^{0.58} \mathbf{Fe} + k_{Fe}^{inorg} \mathbf{Fe}^{1.5} \quad (2)$$

where k_{Fe}^{org} and k_{Fe}^{inorg} are the scavenging rate constants, Det_f is the flux of organic matter in $\text{nmol N m}^{-2} \text{d}^{-1}$, and w_{sink} is the speed of sinking particles in m d^{-1} . The parameter values $k_{Fe}^{org} = 1.0521 \times 10^{-4} (\text{nM N m}^{-3})^{-0.58} \text{d}^{-1}$ and $k_{Fe}^{inorg} = 6.10^{-4} (\text{nM Fe m})^{-0.5} \text{d}^{-1}$ were optimized so that the magnitude and gradient of equatorial iron between 156°E and 110°W give the closest possible match between

Table 1. Lagrangian Sensitivity Experiments^a

No.	Experiment Name	Source Section				
		NGCU	NICU	MC	Recirc	Other src
1	BACK	Back	Back	Back	Obs	Back
2	NGCU-LOW	DFe	Back	Back	Obs	Back
3	NGCU&NICU-LOW	DFe	DFe	Back	Obs	Back
4	NGCU&NICU&MC-LOW	DFe	DFe	DFe	Obs	Back
5	NGCU-HIGH	TDFe	DFe	DFe	Obs	Back
6	NGCU&NICU-HIGH	TDFe	TDFe	DFe	Obs	Back
7	NGCU&NICU&MC-HIGH	TDFe	TDFe	TDFe	Obs	Back
8	NGCU-VAR	Variable	TDFe	Back	Obs	Back
9	NGCU-CST	7.5	TDFe	Back	Obs	Back
10	NGCU&NICU-VAR	Variable	Variable	Back	Obs	Back
11	NGCU&NICU-CST	7.5	7.5	Back	Obs	Back

^aExperiments 1–7 use fixed iron concentration profiles at the source locations to examine the mean EUC iron concentrations. Experiments 8–11 use variable iron concentration profiles at selected sources. NGCU: New Guinea Coastal Undercurrent; NICU: New Ireland Coastal Undercurrent; MC: Mindanao Current; Recirc: recirculation; Other src: for the remaining sections, South of Solomon Islands, North Interior, North of EUC, South of EUC (see Figure S4); Back: averaged background iron profile; DFe: dissolved iron (Figure 1b); TDFe: total dissolved iron profile (Figure 1c); Obs: averaged open ocean iron profile (Figure 1a); Variable: variable iron profile (Figure 2a); and 7.5: time mean TDFe concentration (Figure 2a).

the available observations. Validation and optimization of the Lagrangian model are further described in Texts S4 and S5.

There are four likely sources of iron into the Pacific: (i) sediment resuspension, (ii) hydrothermal vents, (iii) riverine runoff, and (iv) atmospheric dust deposition [Mackey *et al.*, 2002]. Unfortunately, observations available to parameterize the mobilization of iron from marine sediments, riverine, or hydrothermal fluxes are limited [Aumont *et al.*, 2015; Graham *et al.*, 2015; Resing *et al.*, 2015]. Thus, Fe_{src} is based on water column measurements of iron concentrations in this region [Blain *et al.*, 2008; Coale *et al.*, 1996; DiTullio *et al.*, 1993; Fitzwater *et al.*, 1996; Kaupp *et al.*, 2011; Kondo *et al.*, 2012; Mackey *et al.*, 2002; Slemons *et al.*, 2010; Takeda and Obata, 1995; Wu *et al.*, 2011].

Lagrangian particles were released continuously at five sections intersecting the EUC core at 156°E, 165°E, 170°W, 140°W, and 110°W and integrated backward in time (backtracked) until they reached one of the eight predefined source regions (NGCU, NICU, MC, east of Solomon Island, south of EUC, North Interior, north of EUC, and recirculation; Figure 1d). Iron concentrations were then assigned to these particles at the source sections and the iron model (equation (1)) integrated forward in time along the predetermined Lagrangian pathways into and along the EUC. Simulations were integrated offline using velocity, phytoplankton, zooplankton, and detritus outputs from OFAM3-WOMBAT [Oke *et al.*, 2012].

To determine what combination of iron sources might explain the observed iron concentrations along the EUC, seven experiments were performed, with different iron profiles assigned at the source locations, based on observed depth-varying profiles (Figures 1a and 1b). The different profiles assigned in each of the sensitivity experiments are described in Table 1. We examined both dissolved iron (DFe), which is readily bioavailable and total dissolved iron (TDFe), which also includes iron species that could become bioavailable through nonreductive processes [Labatut *et al.*, 2014] or through photochemical reduction when upwelled in the EEP. However, it should be noted that TDFe is thought to contribute very little to biological uptake [Slemons *et al.*, 2010, 2012]. Therefore, DFe and TDFe could be thought of as, respectively, lower and upper bounds on bioavailable iron in the EEP, although we note that lower values of bioavailable iron are possible as some of the dFe may not be bioavailable if bound to organic ligands.

The DFe background profile (Figure 1a) is an average of all the observed iron profiles away from the coast (>500 km) in the tropical Pacific (<5°) (Figure S6, red circles) and represents a typical nutrient profile with minimum values at ~80 m due to biological uptake and a subsequent increase with depth as biological matter remineralizes to the background iron concentration of ~0.6 nM in the open ocean. Iron values are elevated near the surface as a result of atmospheric dust deposition [Johnson *et al.*, 1997]. This profile is also used as an

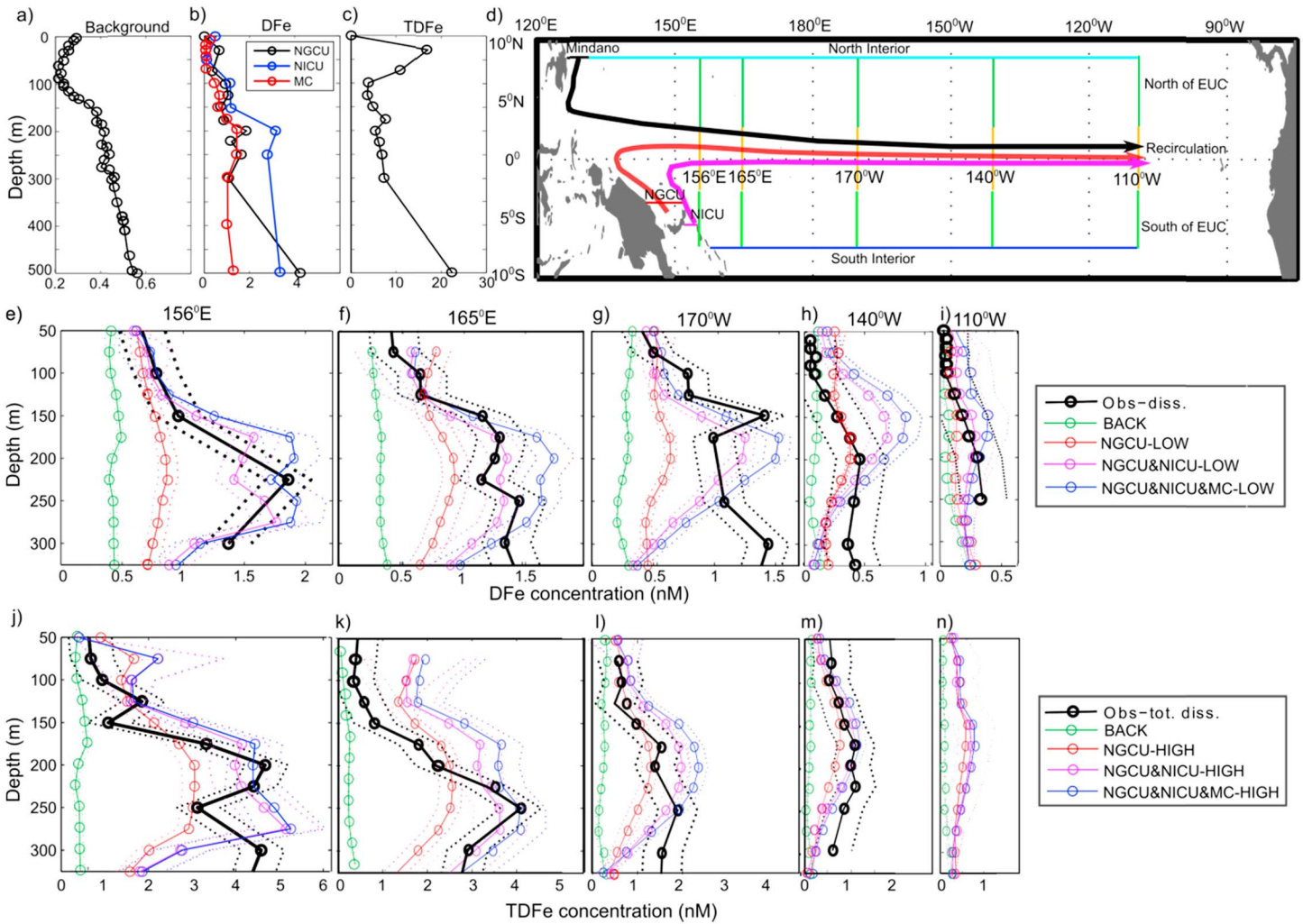


Figure 1. (a) Background (DFe and TDFe), (b) DFe, and (c) TDFe depth profiles imposed during the time constant experiments described in Table 1. In Figure 1b, the DFe profiles are for the NGCU (black), NICU (blue), and Mindanao Current (red). In Figure 1c, the same profile is used for all source regions. (d) Map of EUC iron source and release sections. The source sections are south of the EUC (light green), north of the EUC (dark green), North Interior (cyan), Mindanao Current (black), NGCU (red), NICU (magenta), South Interior (blue), and recirculation (orange). Also shown are mean paths of the NGCU (red), NICU (magenta), and MC (black) to 110°W. The (e–i) DFe and (j–n) TDFe depth profiles for different experiments and observations at 156°E, 165°E, 170°W, 140°W, and 110°W. The observations are based on 2°S–2°N averaged observations from Coale *et al.* [1996], Kaupp *et al.* [2011], and Slemons *et al.* [2010] and the TDFe observations from Mackey *et al.* [2002] and Slemons *et al.* [2010]. The dashed lines indicate the 1 standard deviation spread in simulated iron concentration; a ± 0.2 nM uncertainty for the DFe observations based on several measurements made at 140°W in Coale *et al.* [1996], Kaupp *et al.* [2011], and Slemons *et al.* [2010]; and a ± 0.4 nM uncertainty for TDFe observations based on cruise measurements of Mackey *et al.* [2002] and Slemons *et al.* [2010].

estimated TDFe background profile. This is not ideal but stems from a lack of available open ocean measurements. Further justification for this choice and sensitivity tests around the importance of this assumption are provided in the supporting information S7 and S8.

For the NGCU, DFe and TDFe measurements are available at three stations off the coast of Papua New Guinea and along the NGCU from 6°S to 3.3°S. Here the station at 144°E, 3.3°S is used (Figure 1b, black line) [Slemons *et al.*, 2010]. This has the highest average iron of the three stations and is closest to our source section. The DFe profile for the NICU is from 155°E, 5°S [Slemons *et al.*, 2010], and the Mindanao Current is from 130°E, 7°N (Figure 1b) [Kondo *et al.*, 2007].

TDFe measurements are not available in the NICU or MC. As a result TDFe profile concentrations for the NGCU are used for these two source regions. This is likely to be an overestimate due to the comparatively small landmasses and lack of large rivers compared to New Guinea. The uncertainties associated with using this profile are discussed in Text S7.

Four additional experiments were used to investigate the effect of time-varying sources of iron (Table 1). Due to the lack of an adequate parameterization for sedimentary iron sources, time variability in the iron source is, as far as we know, not taken into account in any global climate model. As in *Gorgues et al.* [2010], the profile of source TDFe concentration is scaled in proportion to the time-varying current strength (Figure 2a). In the case of the NGCU, this results in a depth-averaged TDFe range of 5.5 to 14 nM (mean 7.5 nM).

For both variable experiments (*NGCU-VAR* and *NGCU&NICU-VAR*; Table 1), the prescribed iron concentrations peak during the 1997/1998 and 2002/2003 El Niño events when current strengths are greatest. OFAM3 does not realistically simulate circulation changes for the weak 2004/2005 El Niño [*Qin et al.*, 2015], and consequently, no iron peak is evident in 2005. These experiments were compared to control experiments, where the NGCU and NICU source concentrations are held fixed at the mean value of 7.5 nM (Figure 2a).

3. Results

We begin by examining whether a sole NGCU iron source or combination of iron sources can reproduce the observed equatorial iron concentration distribution. As expected, in the *BACK* experiment, where all sources are set with the background iron profile (Figure 1a), the iron concentrations are lower than observations for both DFe and TDFe (Figures 1e–1n, green versus black lines). All the other experiments exhibit a subsurface iron maximum at 175–275 m at 156°E (Figures 1e and 1j), shoaling to 125–225 m at 140°W (Figures 1h and 1m) in agreement with observations.

With a single DFe or TDFe NGCU source (*NGCU-LOW* and *NGCU-HIGH*; Figures 1e–1n, red lines), the iron content is significantly greater than in the *BACK* experiments. However, both DFe and TDFe are considerably underestimated in the western part of the EUC, until about 170°W for TDFe and 140°W for DFe.

However, with the addition of an elevated NICU source concentration (*NGCU&NICU-LOW* and *NGCU&NICU-HIGH*), the zonal gradient along the EUC is enhanced and the simulated iron concentration maximum increases in better agreement with observation at most sections, that is, DFe peak concentrations of 1.8 nM (156°E) and 1.3 nM (165°E and 170°W) compared with observations of 1.9 nM (156°E) and 1.5 nM (165°E and 170°W) and TDFe peak concentrations of 5.1 nM (156°E) and 1.2 nM (140°W) compared with observations of 4.6 nM (156°E) and 1.1 nM (140°W). *Qin et al.* [2015] demonstrated that in OFAM3 the volume of water entering the EUC from the NGCU and NICU are similar. As such, an elevated iron source from the NICU could significantly enhance the EUC iron concentrations. Interestingly, the NICU is also more efficient in transporting iron to the EEP than the NGCU. At high iron concentration (>0.6 nM), the rate of iron scavenged is proportional to the iron concentration and thus the total amount of iron scavenged from source into the EUC will depend not only on the initial iron concentration but also on the transit time between source and destination. In the model, transit times from source to 110°W are generally shorter for the NICU, with an interquartile range of 321–763 days for the NGCU and 210–595 days for the NICU. As a result, all else being equal, there would be relatively less scavenging along the faster NICU pathway to a given point along the EUC compared to the NGCU pathway. For example, at 170°W, scavenging would lead to a 69% TDFe reduction for NGCU-sourced waters, whereas NICU TDFe would be reduced by only 48% despite starting with similar concentrations of 7.5 nM at the source and similar dilution effects from the other EUC sources (i.e., TDFe concentration is further reduced by 58% to 0.95 nM for NGCU and by 60% to 1.55 nM as a result of dilution; Figure 1l).

If an additional source is added at the MC (DFe: *NGCU&NICU&MC-LOW* and TDFe: *NGCU&NICU&MC-HIGH*), the iron concentration at 165°E and 170°W becomes overestimated (Figures 1f, 1g, 1k, and 1l). However, the relatively small increase in iron concentration between experiments with (*NGCU&NICU&MC-LOW* and *HIGH*) and without (*NGCU&NICU-LOW* and *HIGH*) elevated MC iron indicates that this source is less important than the NGCU and NICU sources (Figures 1e–1n). This can be explained by the much longer median transit time from the MC to the EUC (463 days to 170°W) compared to the NICU (126 days to 170°W), which provides more time for iron scavenging. The relatively longer transit time from the MC to the EUC is because MC is situated further eastward than the NICU and the waters circulate around the stationary Halmahera eddy [*Qin et al.*, 2015].

The observed peak in iron concentrations in the EUC can be reproduced by arbitrarily raising the average NGCU concentration to 19.8 nM (from our estimated value of 7.5 nM), which would be slightly higher than concentrations reported along other similar continental shelf regions (e.g., 15.5 nM [*Bruland et al.*, 2005]), although higher TDFe concentrations have been identified off the Coast of Peru, where the sediments are

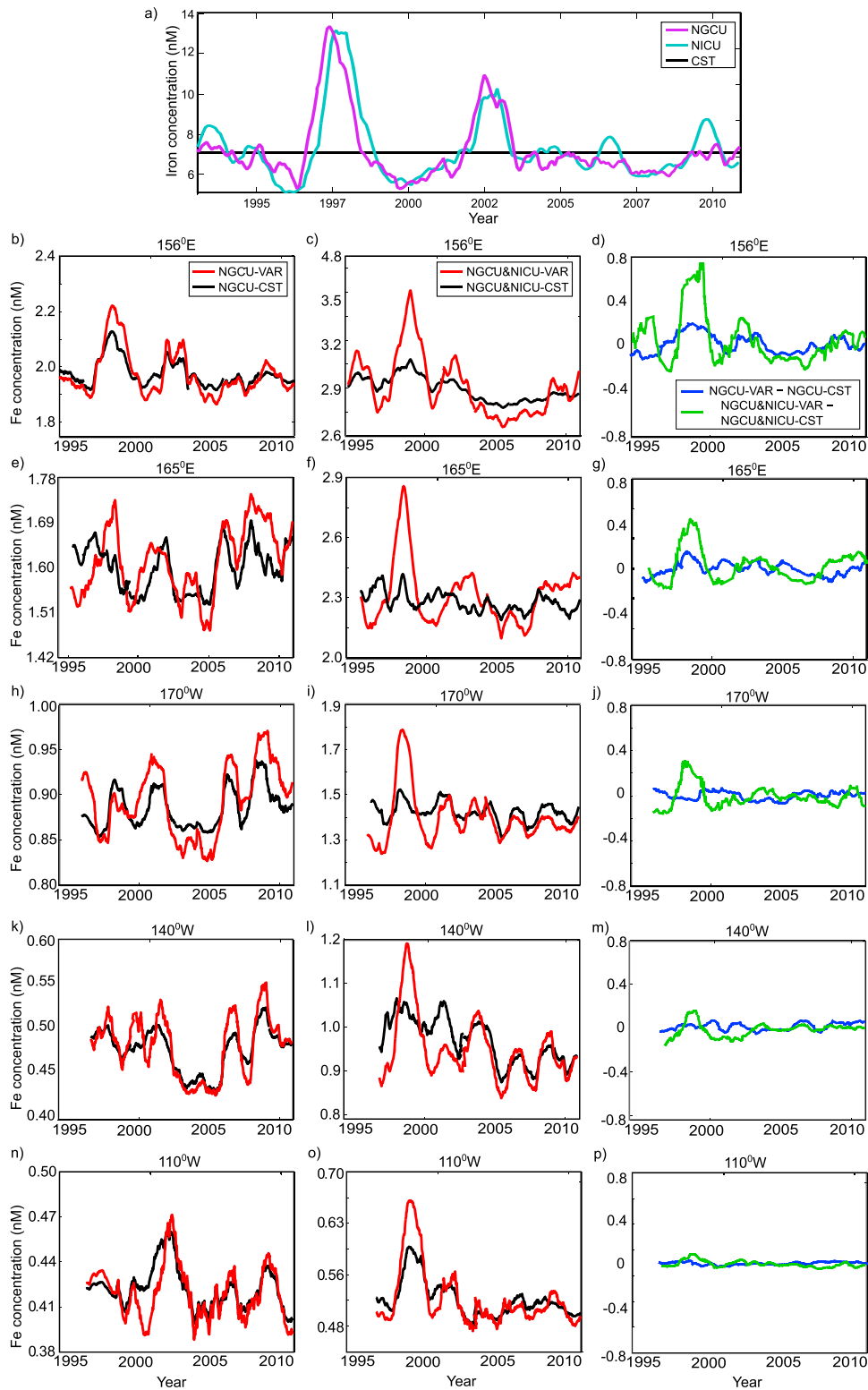


Figure 2. (a) Prescribed time constant (black, CST) and variable source region iron concentrations for NGCU (purple) and NICU (green) used in VAR experiments (Table 1). The TDFe concentration at (b–d) 156°E, (e–g) 156°E, (h–j) 170°W, (k–m) 140°W, and (n–p) 110°W for constant (black) and variable (red) iron concentrations. The first column is for experiments NGCU-CST and NGCU-VAR and the second column for NGCU&NICU-CST and NGCU&NICU-VAR. The third column shows the differences between the variable and constant experiments (NGCU in blue and NGCU&NICU in green). All time series are based on an average of all the particles transiting between source and release sections (this corresponds to a depth range of ~100–275 m in the western basin shoaling to ~50–200 m in the eastern basin). Time series have been smoothed with a 180 day running mean.

reduced [Chever *et al.*, 2015]. However, this is well beyond the range of observed iron within the NGCU core (Figure 1c). Similarly, the low equatorial iron concentrations simulated with the elevated NGCU-only experiments could be related to underestimated contributions from sources away from the western boundaries (e.g., via thermocline water convergence). However, even if we raise all interior water concentrations to the maximum open ocean observed concentrations of 1 nM [Gorgues *et al.*, 2010], equatorial iron concentrations are still underestimated (Text S7).

While numerical experiments performed by Ryan *et al.* [2006] suggest that a variable iron supply can modulate primary productivity in the EEP on interannual time scales, Gorgues *et al.* [2010] find that a variable NGCU iron signal is damped before reaching the upwelling regions due to nonlinear scavenging at high iron concentrations. Here we test whether an additional enhanced iron concentration from the NICU, with its shorter transit pathway and similar water volume contribution to the NGCU, may explain the EEP blooms.

Iron concentration variability in the EUC can result from changes in the initial iron concentration at the source but also from circulation variability. In particular, changes in tropical Pacific circulation associated with ENSO modify the proportion of water from each EUC source as well as water mass transit times [Qin *et al.*, 2015]. This in turn alters the amount of iron scavenging. Comparing the simulation with a time-varying NGCU source iron concentration (NGCU-VAR) with a control simulation where the NGCU iron concentration is held constant (NGCU-CST), we find that high variability in EUC iron concentration exists even when the source concentration is fixed. Moreover, when the NGCU source iron concentration is varied, any associated variability quickly diminishes along the EUC becoming similar to the constant NGCU iron simulation (Figures 2b and 2e). The lack of any significant difference between the constant and variable experiments in the eastern Pacific (110°W; Figures 2n and 2p) results from the large dilution of NGCU water, making up the EUC by water coming from interior sources. Interior sources include the sections south and north of the EUC (light and dark green), North Interior (cyan), South Interior (blue), and recirculation (orange; Figure 1d). At 110°W, only 5% of particles are sourced from the NGCU while interior sources make up to 82% of EUC particles. In addition, coherent pulses of high NGCU iron (Figure 2a) are eroded by the time they reach the eastern Pacific as water parcels have very different transit times from the NGCU source region (interquartile range 321 to 663 days).

In contrast, for the combined variable NGCU and NICU iron source (NGCU&NICU-VAR), the 1997 and 2002 iron peaks persist to the eastern Pacific as a result of elevated source iron concentrations (Figure 2o). This is because the two currents vary in phase, with a stronger current during El Niño events, thereby enhancing the iron anomaly entering the EUC. Even at 110°W where the combined NGCU and NICU are responsible for only 16% of EUC water, the iron pulse from the large 1997 El Niño is evident, although the smaller 2002 pulse is no longer present. Experiment NGCU&NICU-VAR exhibits an iron peak of 0.65 nM in 1998/1999 (Figure 2o), which is ~12% higher than the time constant NGCU&NICU-CST iron peak of 0.58 nM.

For the sole NGCU variable source, there is a significant correlation between the source concentration (Figure 2a) and the iron concentration at 156°E and 165°E ($r=0.39$ and 0.22 , respectively, with a lag of ~180 days consistent with modal transit times). Further east, there is no significant correlation despite the clear persistence of the large 1997 peak in iron concentration (Figures 2k and 2n). In contrast, the associated correlation for the NGCU&NICU-VAR remains significant at all sections decreasing from $r=0.55$ at 156°E with a lag of 102 days to $r=0.4$ at 110°W with a lag of 410 days, again consistent with the interquartile range of transit times of 18–194 days at 156°E and 210–595 days at 110°W (Table S2). These results are also in agreement with Ryan *et al.* [2006], where the EEP blooms were observed to occur about 9–13 months after the maximum NGCU shoaling and intensification (Table S2).

The increased delivery of iron to the EEP is highly dependent on the transit times from the NGCU and NICU to the EUC, which exhibits large variability due to the circulation in the western Pacific eddies [Qin *et al.*, 2015]. Our experiments suggest that a doubling of the western equatorial Pacific iron source as well as shorter transit times from the NICU leads to a significant increase in iron delivery to the EEP, e.g., during the 1997/1998 El Niño event. Thus, it requires a combined NGCU and NICU iron delivery to enhance surface productivity in the EEP.

4. Conclusions

The Lagrangian iron model developed and used here has a number of advantages over traditional Eulerian source removal iron models [Moore and Braucher, 2008; Tagliabue *et al.*, 2009, 2010, 2014] for investigating

the role of iron sources and transport. Backtracking of particles from their final destination makes it possible to isolate the water mass pathways important for a particular region. This subsequently allows highly efficient forward integration of tracer evolution along these trajectories, without the need to make calculations at all spatial points as required in an Eulerian simulation. As such, multiple sensitivity experiments can be run with small computational cost. This methodology means that we can easily optimize parameters or change parameterizations (e.g., for scavenging) so as to minimize tracer biases relative to available observations. We can also easily modify source water concentrations, including using observed values, to test the importance of different water mass pathways in modulating destination tracer concentrations.

Several studies assume that the NGCU is the sole iron source due to its proximity to a large landmass with a major river and the fact that a large portion of the EUC derives from the NGCU [Gorgues *et al.*, 2010; Ryan *et al.*, 2006]. Despite uncertainties in the magnitude and variability of a bioavailable NGCU iron, an enhanced NGCU iron concentration has been widely utilized in sensitivity studies of equatorial productivity [Gorgues *et al.*, 2010; Ryan *et al.*, 2006; Slemons *et al.*, 2009; Vichi *et al.*, 2008; Wells *et al.*, 1999].

However, a sole NGCU source underestimates both DFe and TDFe (which we use as a proxy for the upper limit on bioavailable iron in the EEP) observed along the EUC (Figures 1e–1i). The rapid decrease in iron concentration from the NGCU source results from (i) high levels of scavenging that occur when iron concentrations are much greater than the background concentration and (ii) dilution by low iron content interior water masses. By including an additional NICU iron source, EUC concentrations are more consistent with observed vertical distributions along the equator. These results apparently contradict Vichi *et al.* [2008], who found realistic equatorial iron concentrations with a sole NGCU source. However, their elevated source iron concentrations were imposed over a larger continental shelf area that also included flow from the NICU. The relatively coarse resolution of their general circulation model (2° with a finer mesh of 0.5° at low latitudes) makes it difficult to distinguish NGCU and NICU.

Ryan *et al.* [2006] hypothesized that an enhancement of volume transport and iron concentration in the NGCU during El Niño events could subsequently lead to elevated western Pacific iron. However, in agreement with Gorgues *et al.* [2010], we find that elevated iron from a NGCU source alone is quickly scavenged and diluted as it propagates westward. In addition, any coherent pulse of iron becomes increasingly eroded by the spread in transit times, resulting from the varied Lagrangian iron particle trajectories [Qin *et al.*, 2015].

As the LLWBCs covary, western Pacific iron pulses associated with El Niño events are considerably larger with combined NGCU and NICU sources. Indeed, the elevated iron injection associated with the 1997/1998 El Niño manifests as 30% higher TDFe concentration in the EEP ~13 months later (Figure 2o). This is consistent with a delay of about 1 year between LLWBC intensification and the EEP productivity response reported in Ryan *et al.* [2006]. The lack of an additional NICU iron source may therefore explain why Gorgues *et al.* [2010] found no improvement in the simulation of EEP blooms in their experiments that relied solely on a variable NGCU source. While the large 1997/1998 iron pulse can be tracked across the Pacific in our experiment, this is not the case for smaller ENSO events. Despite elevated source iron concentration, the combined effect of strong scavenging and large variability in particle transit times [Qin *et al.*, 2015] from both sources means that no coherent change is evident in the eastern Pacific.

The need for additional iron sources to explain mean equatorial iron concentrations and the link between source variability and EEP productivity suggest that additional regional iron observations are critically needed to better quantify iron source contributions.

Acknowledgments

We would like to thank R. Matear for providing the OFAM3-WOMBAT data. This project is supported by the Australian Research Council and the National Computational Infrastructure. E.v.S. and L.M. are supported by the Australian Research Council under grants DE130101336 and DE150100107. The data for this paper are available by contacting the corresponding author L. Menviel (l.menviel@unsw.edu.au). We thank M. Vichi and the anonymous reviewer whose comments helped improve and clarify this manuscript.

References

- Aumont, O., C. Ethé, A. Tagliabue, L. Bopp, and M. Gehlen (2015), PISCES-v2: An ocean biogeochemical model for carbon and ecosystem studies, *Geosci. Model Dev. Discuss.*, 8(2), 1375–1509.
- Blain, S., S. Bonnet, and C. Gieue (2008), Dissolved iron distribution in the tropical and subtropical South Eastern Pacific, *Biogeosciences*, 5(1), 269–280.
- Bruland, K. W., E. L. Rue, G. J. Smith, and G. R. DiTullio (2005), Iron, macronutrients and diatom blooms in the Peru upwelling regime: Brown and blue waters of Peru, *Mar. Chem.*, 93(2), 81–103.
- Chavez, F. P., P. G. Strutton, G. E. Friederich, R. A. Feely, G. C. Feldman, D. G. Foley, and M. J. McPhaden (1999), Biological and chemical response of the equatorial Pacific Ocean to the 1997–98 El Niño, *Science*, 286(5447), 2126–2131.
- Chever, F., O. J. Rouxel, P. L. Croot, E. Ponzevera, K. Wuttig, and M. Auro (2015), Total dissolvable and dissolved iron isotopes in the water column of the Peru upwelling regime, *Geochim. Cosmochim. Acta*, 162, 66–82.

- Christian, J. R., M. A. Verschell, R. Murtugudde, A. J. Busalacchi, and C. R. McClain (2002), Biogeochemical modelling of the tropical Pacific Ocean. I: Seasonal and interannual variability, *Deep Sea Res., Part II*, 49(1–3), 509–543.
- Coale, K. H., S. E. Fitzwater, R. M. Gordon, K. S. Johnson, and R. T. Barber (1996), Control of community growth and export production by upwelled iron in the equatorial Pacific Ocean, *Nature*, 379(6566), 621–624.
- DiTullio, G. R., D. A. Hutchins, and K. W. Bruland (1993), Interaction of iron and major nutrients controls phytoplankton growth and species composition in the tropical North Pacific Ocean, *Limnol. Oceanogr.*, 38(3), 495–508.
- Fitzwater, S. E., K. H. Coale, R. M. Gordon, K. S. Johnson, and M. E. Ondrusek (1996), Iron deficiency and phytoplankton growth in the equatorial Pacific, *Deep Sea Res., Part II*, 43(4), 995–1015.
- Galbraith, E. D., A. Gnanadesikan, J. P. Dunne, and M. R. Hiscock (2010), Regional impacts of iron-light colimitation in a global biogeochemical model, *Biogeosciences*, 7(3), 1043–1064.
- Gordon, R. M., K. H. Coale, and K. S. Johnson (1997), Iron distributions in the equatorial Pacific: Implications for new production, *Limnol. Oceanogr.*, 42, 419–431.
- Gorgues, T., C. Menkes, L. Slemmons, O. Aumont, Y. Dandonneau, M. H. Radenac, S. Alvain, and C. Moulin (2010), Revisiting the La Niña 1998 phytoplankton blooms in the equatorial Pacific, *Deep Sea Res., Part I*, 57(4), 567–576.
- Graham, R. M., A. M. De Boer, E. van Sebille, K. E. Kohfeld, and C. Schlosser (2015), Inferring source regions and supply mechanisms of iron in the Southern Ocean from satellite chlorophyll data, *Deep Sea Res., Part I*, 104, 9–25, doi:10.1016/j.dsr.2015.05.07.
- Johnson, G., and M. J. McPhaden (1999), Interior pycnocline flow from the subtropical to the equatorial Pacific Ocean, *J. Phys. Oceanogr.*, 29(12), 3073–3089.
- Johnson, K. S., R. M. Gordon, and K. H. Coale (1997), What controls dissolved iron concentrations in the world ocean?, *Mar. Chem.*, 57(3), 137–161.
- Kaupp, L. J., C. I. Measures, K. E. Selph, and F. T. Mackenzie (2011), The distribution of dissolved Fe and Al in the upper waters of the eastern equatorial Pacific, *Deep Sea Res., Part II*, 58(3–4), 296–310.
- Kondo, Y., S. Takeda, and K. Furuya (2007), Distribution and speciation of dissolved iron in the Sulu Sea and its adjacent waters, *Deep Sea Res. Part II: Top. Stud. Oceanogr.*, 54(1–2), 60–80.
- Kondo, Y., S. Takeda, and K. Furuya (2012), Distinct trends in dissolved Fe speciation between shallow and deep waters in the Pacific Ocean, *Mar. Chem.*, 134, 18–28.
- Labatut, M., F. Lacan, C. Pradoux, J. Chmieleff, A. Radic, J. W. Murray, F. Poitrasson, A. Johansen, and F. Thil (2014), Iron sources and dissolved-particulate interactions in the seawater of the western equatorial Pacific, iron isotope perspectives, *Global Biogeochem. Cycles*, 28, 1044–1065, doi:10.1002/2014GB004928.
- Mackey, D. J., J. E. O'Sullivan, and R. J. Watson (2002), Iron in the western Pacific: A riverine or hydrothermal source for iron in the Equatorial Undercurrent?, *Deep Sea Res., Part I*, 49(5), 877–893.
- Moore, J. K., and O. Braucher (2008), Sedimentary and mineral dust sources of dissolved iron to the world ocean, *Biogeosciences*, 5(3), 631–656.
- Oke, P. R., D. A. Griffin, A. Schiller, R. J. Matear, R. Fiedler, J. Mansbridge, A. Lenton, M. Cahill, M. A. Chamberlain, and K. Ridgway (2012), Evaluation of a near-global eddy-resolving ocean model, *Geosci. Model Dev. Discuss.*, 5(4), 4305–4354.
- Paris, C. B., J. Helgers, E. van Sebille, and A. Srinivasan (2013), Connectivity Modeling System: A probabilistic modeling tool for the multi-scale tracking of biotic and abiotic variability in the ocean, *Environ. Modell. Software*, 42, 47–54.
- Pichler, T., J. Veizer, and G. E. M. Hall (1999), The chemical composition of shallow-water hydrothermal fluids in Tutum Bay, Ambitle Island, Papua New Guinea and their effect on ambient seawater, *Mar. Chem.*, 64(3), 229–252.
- Qin, X., A. Sen Gupta, and E. van Sebille (2015), Variability in the origins and pathways of Pacific Equatorial Undercurrent water, *J. Geophys. Res. Oceans*, 120, 3113–3128, doi:10.1002/2014JC010549.
- Radic, A., F. Lacan, and J. W. Murray (2011), Iron isotopes in the seawater of the equatorial Pacific Ocean: New constraints for the oceanic iron cycle, *Earth Planet. Sci. Lett.*, 306(1), 1–10.
- Resing, J. A., P. N. Sedwick, C. R. German, W. J. Jenkins, J. W. Moffett, B. M. Sohst, and A. Tagliabue (2015), Basin-scale transport of hydrothermal dissolved metals across the South Pacific Ocean, *Nature*, 523(7559), 200–203.
- Ryan, J. P., I. Ueki, Y. Chao, H. Zhang, P. S. Politto, and F. P. Chavez (2006), Western Pacific modulation of large phytoplankton blooms in the central and eastern equatorial Pacific, *J. Geophys. Res.*, 111, G02013, doi:10.1029/2005JG000084.
- Slemmons, L., T. Gorgues, O. Aumont, C. Menkes, and J. W. Murray (2009), Biogeochemical impact of a model western iron source in the Pacific Equatorial Undercurrent, *Deep Sea Res., Part I*, 56(12), 2115–2128.
- Slemmons, L., J. W. Murray, J. Resing, B. Paul, and P. Dutrieux (2010), Western Pacific coastal sources of iron, manganese, and aluminum to the Equatorial Undercurrent, *Global Biogeochem. Cycles*, 24, GB3024, doi:10.1029/2009GB003693.
- Slemmons, L., B. Paul, J. Resing, and J. W. Murray (2012), Particulate iron, aluminum, and manganese in the Pacific Equatorial Undercurrent and low latitude western boundary current sources, *Mar. Chem.*, 142, 54–67.
- Tagliabue, A., L. Bopp, and O. Aumont (2009), Evaluating the importance of atmospheric and sedimentary iron sources to Southern Ocean biogeochemistry, *Geophys. Res. Lett.*, 36, L13601, doi:10.1029/2009GL038914.
- Tagliabue, A., L. Bopp, J.-C. Dutay, A. R. Bowie, F. Chever, P. Jean-Baptiste, E. Bucciarelli, D. Lannuzel, T. Remenyi, and G. Sarthou (2010), Hydrothermal contribution to the oceanic dissolved iron inventory, *Nat. Geosci.*, 3(4), 252–256, doi:10.1038/ngeo818.
- Tagliabue, A., R. G. Williams, N. Rogan, E. P. Achterberg, and P. W. Boyd (2014), A ventilation-based framework to explain the regeneration-scavenging balance of iron in the ocean, *Geophys. Res. Lett.*, 41, 7227–7236, doi:10.1002/2014GL061066.
- Tagliabue, A., et al. (2015), How well do global ocean biogeochemistry models simulate dissolved iron distributions?, *Global Biogeochem. Cycles*, 30, 149–174, doi:10.1002/2015GB005289.
- Takeda, S., and H. Obata (1995), Response of equatorial Pacific phytoplankton to subnanomolar Fe enrichment, *Mar. Chem.*, 50(1), 219–227.
- Vichi, M., S. Masina, and F. Nencioli (2008), A process-oriented model study of equatorial Pacific phytoplankton: The role of iron supply and tropical instability waves, *Prog. Oceanogr.*, 78(2), 147–162.
- Wells, M. L., G. K. Vallis, and E. A. Silver (1999), Tectonic processes in Papua New Guinea and past productivity in the eastern equatorial Pacific Ocean, *Nature*, 398(6728), 601–604.
- Wu, J., M. L. Wells, and R. Rember (2011), Dissolved iron anomaly in the deep tropical–subtropical Pacific: Evidence for long-range transport of hydrothermal iron, *Geochim. Cosmochim. Acta*, 75(2), 460–468.